PERGAMON

Chemical Engineering Science 57 (2002) 887–900

Chemical Engineering Science

www.elsevier.com/locate/ces

Development of a comprehensive free radical photopolymerization model incorporating heat and mass transfer effects in thick films

Michael D. Goodner[a, 1], Christopher N. Bowman[a,b, *]

[a] *Department of Chemical Engineering, University of Colorado at Boulder Engineering Center, Campus Box 424, Boulder, CO 80309-0424, USA*

[b] *Department of Restorative Dentistry, University of Colorado Health Sciences Center, Denver, CO, USA*

Received 7 February 2000; accepted 18 June 2001

Abstract

A comprehensive kinetic model describing photopolymerization is developed which allows variation of temperature, species concentrations, and light intensity through the thickness of a photopolymerized film. Heat and mass transfer effects are included, as is the generation of heat by both reaction and light absorption. In addition to initiation, propagation, and termination mechanisms, both primary radical termination and inhibition are incorporated into the model. The possible presence and diffusion of an inert solvent are also accounted for. Thus, the model is useful for examining complex polymerization kinetics and behavior in industrially and commercially important thick film photopolymerizations, such as the curing of contact lenses, dental restorative materials, photolithographic resists, and optoelectronic coatings. The comprehensive model is used to predict polymerization rate, temperature, and conversion profiles in a variety of systems. The effects of heat generation and the thermal boundary conditions are explored, with the result that heat generation in thick samples leads to greatly increased conversions approaching 100 percent. Increased temperature in these samples also may lead to the appearance of two rate maxima, with the first due to the temperature increase and the second caused by the autoacceleration process. The magnitude of the temperature increase, along with the resultant effects, is more pronounced in insulated systems.

Keywords: Heat transfer; Kinetics; Mass transfer; Mathematical modeling; Photopolymerization; Simulation

1. Introduction

Photopolymerization products dominate the specialty polymers market. Both cationic and free-radical photopolymerizations allow a wide variety of monomers to be polymerized individually or in the presence of comonomers, which in turn allows a great range of materials to be produced. Selection of the proper monovinyl monomers, which form linear polymers upon reaction, and multifunctional monomers, which form crosslinked polymeric networks, allows the optical, mechanical, and physicochemical properties of the resultant polymeric material to be tailored by the formulation scientist. The fact that polymerization generally proceeds only in areas illuminated with radiation allows facile spatial and temporal control of the reaction through the use of photomasks, focused illumination sources, and limited duration exposures. Additionally, photopolymerizations can be carried out at ambient temperatures and in solvent-free or solvent-poor systems, leading to low energy costs and minimal environmental impact. The great control over polymer properties, along with the relative simplicity of the polymerization process, leads to the wealth of photopolymers currently marketed by both major chemical conglomerates and small specialty companies.

Materials produced through free-radical photopolymerization span the entire range covered by photopolymers in general. Optoelectronic applications such as optical fiber and video disc coatings, photolithographic resists, and aspherical lens production typically utilize highly crosslinked photopolymers produced through

* Corresponding author. Tel.: +1-303-492-3247; fax: +1-303-492-4341.

E-mail address: christopher.bowman@colorado.edu (C. N. Bowman).

[1] Present address: Intel Corporation, 5200 NE Elam Young Parkway, M/S RA2-372, Hillsboro, OR 97124, USA.

0009-2509/02/$ - see front matter
PII: S0009-2509(01)00287-1

free-radical reactions (Kloosterboer, 1988; Decker, 1996). Biomedical devices are also produced via radical photopolymerization techniques, ranging from loosely crosslinked hydrogels used as drug delivery systems, absorption resins, and contact lenses (Kannurpatti, Peiffer, Guymon, & Bowman, 1996; Peiffer, 1997) to the composite filled polymers used for dental restorative materials (Anseth, Newman, & Bowman, 1995). These examples are but several among the numerous materials commonly produced through free-radical photopolymerization.

While photopolymerization allows a range of materials to be produced and has a number of advantages compared to other types of polymerization processes, there are several constraints that must be addressed when implementing photopolymerization technology. The most important caveat is that photopolymerization is used primarily for thin films, as a number of detrimental effects increase with sample thickness. As light from the illumination source penetrates the sample, it is absorbed by the initiating species (along with monomer and polymer moieties in some systems), causing a decrease in light intensity with depth into the sample. This gradient in light intensity causes gradients in polymerization rate and double bond conversion. The sample surface closest to the illumination source will have a higher polymerization rate and conversion due to the increased rate of photoinitiation, giving an inhomogeneous sample for 'optically thick' films (Goodner & Bowman, 1998). Photobleaching initiators, which have an greatly decreased absorbance after photolysis, and high powered, focused laser sources can be used to mitigate these problems, although their use introduces other vexations, such as decreased initiation efficiencies for photobleaching initiators or increased heat generation caused by laser illumination.

A light intensity gradient in a thick sample can also lead to heat and mass transfer-related effects. Areas which experience higher light intensities will generally have a greater temperature rise during polymerization, resulting from the increased heat production effected both by the absorbance of the incident light and by the exothermic polymerization reaction itself. A variation in double bond conversion also produces a monomer concentration gradient within the sample. While this gradient may not have noticeable effects in solvent-free systems, the presence of a solvent allows monomer to diffuse more easily from high concentration, low conversion regions to low concentration, high conversion locales, which leads to a spatially inhomogeneous material.

Heat and mass transfer-related effects can also arise in the absence of a light intensity gradient. During a photopolymerization, considerable heat is released due to the exothermic nature of the reaction. If a film is cured in contact with insulating materials (such as a foamed plastic or stagnant air), the temperature in the sample will increase considerably, as the adiabatic temperature rise for common monomers can easily exceed 200°C. This temperature increase, in turn, influences the polymerization kinetics and the viscosity of the curing film. If the film is cured in contact with conducting materials, such as metals, heat is transferred to the substrate, and temperature gradients can arise between the interior and the surfaces of the sample. Likewise, the boundary conditions can affect mass transfer characteristics. For example, if the polymerization is performed in a volatile solvent, the presence of a free surface allows evaporation of the solvent over the course of the reaction. Similarly, a permeable surface can allow diffusion of molecular oxygen, a polymerization inhibitor, into the sample if the process is performed in air.

While heat and mass transfer in photopolymerized films can have numerous effects on the cure behavior and resultant properties of the polymer, research reported in the open literature has dealt almost exclusively with the over-simplified case of homogeneous, thin-film polymerization behavior. Experimental studies have investigated effects on the periphery of some of the aforementioned issues but have not addressed them directly. For example, extra mobility afforded by heating the sample during or after polymerization has been shown to increase the ultimate conversion (Kloosterboer, van de Hei, Gossink, & Dortant, 1984; Broer, Mol, & Challa, 1991), but the rate of heat input and the uniformity of temperature throughout the sample were not studied. Similarly, oxygen inhibition in photopolymerized films and the minimization of its impact have received a great deal of attention (Decker, Faure, Fizet, & Rychla, 1979; Decker & Jenkins, 1985; Decker & Elzaouk, 1995). However, the focus has been on consumption of oxygen already present in the film at the start of the cure process while neglecting the diffusion of oxygen into the film during the photopolymerization.

Likewise, modeling studies have, for the most part, left heat and mass transfer effects in photopolymerization unaddressed. Local diffusion of monomer and radicals is considered inherently in modeling diffusion-controlled polymerization kinetics (Marten & Hamielec, 1978, 1982), and the related reaction-diffusion termination mechanism (Buback, 1990; Anseth & Bowman, 1993; Buback, Huckestein, & Russell, 1994; Panke, 1995). However, the macroscopic diffusion of monomer, solvent, or inhibitor that can lead to concentration gradients across a film's thickness have been left unstudied. One of the most comprehensive free-radical polymerization models to date incorporates a wealth of features, such as chain transfer and multiple initiators, but neglects completely both heat and mass transfer in polymerizing sample (Gao & Penlidis, 1996).

To gain a proper understanding of the effects that heat and mass transfer can have on photopolymerization processes and to minimize deleterious polymerization behavior through process optimization, the current void in the published research must be filled. This work moves

toward this goal by developing a comprehensive kinetic model incorporating diffusion controlled propagation and termination kinetics in combination with heat and mass transfer effects. The model is based on previously developed kinetic models which account for variation of light intensity in one spatial dimension (Goodner & Bowman, 1998), primary radical termination (Goodner & Bowman, 1999), and both diffusion-controlled and reaction-diffusion controlled propagation and termination kinetics (Marten & Hamielec, 1978, 1982; Anseth & Bowman, 1993). The model is expanded to include heat generation by reaction and light absorption, heat transfer within the sample and between the sample and the surrounding environment, the presence of solvent and inhibitor, the diffusion of mobile species within the sample, and the diffusion of inhibitor from the environment into the sample. The model then is used to predict conversion, rate, and temperature as a function of both depth and time in a typical polymerization system to show the utility of the model. Next, the effects of the thermal boundary conditions and heat generation on the polymerization behavior are investigated, and the variation of cure time with the incident light intensity also is explored.

2. Model development

In general, successful photopolymerization models are based on the three primary reaction mechanisms occurring during the polymerization: initiation, propagation, and termination. The model developed here, which is based on two previously presented models (Goodner & Bowman, 1998, 1999), is no exception. Expanding the basic mechanisms to account for features such as primary radical termination, inhibition, and inhibited chain reinitiation gives the following scheme:

Initiation

$$I \xrightarrow{h\nu} 2R\bullet, \tag{1}$$

$$R\bullet + M \xrightarrow{k_i} P_1\bullet, \tag{2}$$

$$P_nZ\bullet + M \xrightarrow{k_i'} P_{n+1}\bullet. \tag{3}$$

Propagation

$$P_n\bullet + M \xrightarrow{k_p} P_{n+1}\bullet. \tag{4}$$

Termination

$$P_n\bullet + P_m\bullet \xrightarrow{k_t} P_{n+m}/P_n + P_m, \tag{5}$$

$$P_n\bullet + R\bullet \xrightarrow{k_{tp}} P_n. \tag{6}$$

Inhibition

$$P_n\bullet + Z \xrightarrow{k_z} P_nZ\bullet. \tag{7}$$

In this reaction mechanism, Eq. (1) is the photolysis of initiator, I, to give two primary radicals, $R\bullet$, which in this work are assumed to be equivalent with respect to their reactivity and mobility. The rate of consumption of initiator is determined by the absorption of light and is given by the following equation:

$$R_{\text{init}} = \frac{\varepsilon I c_I}{E'}, \tag{8}$$

where ε is the molar absorptivity of the initiator, I is the light intensity (in mW/cm^2) and c_I is the photoinitiator concentration. E' is the energy per mole of photons and is dependent on the wavelength of the illumination source. This value is required to convert from the power density given by I to a molar rate for the decomposition of initiator.

The second step of initiation is the chain initiation process, shown by Eq. (2). In this reaction, a primary radical reacts with monomer, M, to form a growing polymer chain one repeat unit in length, $P_1\bullet$. The rate of this reaction is determined by the kinetic constant for chain initiation, k_i. A second type of chain initiation is given by Eq. (3): reinitiation of inhibited chains. In this reaction, an inhibited chain, $P_nZ\bullet$, reacts with monomer to reform an actively growing chain. The kinetic constant for reinitiation, k_i' will in general be different than k_i; in fact, the value of k_i' in most systems is either considerably lower (several to many orders of magnitude) than k_i or is considered to be zero.

The propagation reaction is represented by a single reaction (4), and the kinetic constant for propagation is k_p. Chain termination occurs through two different mechanisms. Bimolecular termination (5) occurs when two growing radical chains come together and react to form dead polymer; this reaction can either occur by combination (forming one polymer chain) or disproportionation (forming two chains). While the mode of termination significantly affects the molecular weight in linear polymer-forming systems, the polymerization kinetics in crosslinked systems, which are predominant in commercial photopolymer applications, are not influenced significantly by the termination mode. Thus, the bimolecular termination reaction will be lumped into a single reaction having kinetic constant k_t. The second termination mechanism is primary radical termination (6), in which a primary radical reacts with a growing polymer chain to form dead polymer. The kinetic constant for this process, k_{tp}, will in general be different from the bimolecular k_t, as the two reactions have different chemistry and different species mobilities involved in the termination process.

The last reaction occurring during the polymerization is chain inhibition (7). In this process, an inhibitor species, Z, such as molecular oxygen or an intentionally added inhibitor, reacts with a growing chain to form a relatively

unreactive species. The kinetic constant for this reaction is k_z.

To adapt this scheme for a model incorporating spatial variations, the same methodology as used in Goodner and Bowman (1998) is employed. Mathematically, the sample is divided into thin slices over which light intensity, species concentrations and temperature do not vary greatly. The species balances implied by Eqs. (1)–(7) are then solved in each slice at each sequential time step. However, this comprehensive model additionally incorporates mass transfer into the species balance equations to allow diffusion of mobile species between neighboring slices and also adds an energy balance term to treat heat generation and heat transfer within the sample. Description of these terms follows in subsequent sections.

The model based on Eqs. (1)–(8) including spatial variations incorporates several assumptions. Summarized for clarity, they are

- initiation is assumed to generate two primary radicals of equal mobility and reactivity;
- propagation, termination, and inhibition are assumed to be independent of chain length;
- bimolecular termination is characterized by a lumped k_t parameter that accounts for both combination and disproportionation;
- illumination is monochromatic;
- light intensity, concentrations, and temperature do not vary significantly over the length scale of the spatial discretization;
- volume of each slice used in the model (and therefore the entire system) does not vary significantly over the course of the reaction.

2.1. The energy balance

In the polymerizing sample, heat can be generated in two ways: by the exothermic polymerization reaction and by light absorption by the photoinitiator or its decomposition products (most monomers and polymers tend to be transparent in the ultraviolet wavelengths commonly used and therefore do not generate heat via absorption). In addition to generation, the species balance must incorporate heat transfer throughout the film. Accordingly, the general energy balance reads as follows:

$$\rho c_p \frac{\mathrm{d}T}{\mathrm{d}t} = k\frac{\mathrm{d}^2T}{\mathrm{d}z^2} - \Delta H \left.\frac{\mathrm{d}M}{\mathrm{d}t}\right|_{rxn} + \varepsilon I c_I^*. \tag{9}$$

In this equation, the left-hand side term represents accumulation. ρ and c_p are the density and mass specific heat, respectively. The first right-hand side term is transfer of heat by conduction. k is the thermal conductivity of the sample, and z is the spatial coordinate, i.e., depth into the film. The second term shows the heat generation by reaction. ΔH is the heat of polymerization, and the derivative $\mathrm{d}M/\mathrm{d}t$ represents the consumption of monomer through all reactions (chain initiation, propagation, and reinitiation of inhibited chains) in each slice. The last term shows the energy generation through absorption of light where ε is the molar absorptivity, I is the incident light intensity in the slice, and c_I^* is the concentration of all initiator moieties in the slice. This term accounts for initiator, primary radicals, and initiator fragments incorporated into polymer chains. The factor c_I^* will be elaborated on in the following section on the species balance equations. The reader may note that the absorption term assumes that all absorbed energy is converted to heat. Some energy does go to bond cleavage, which produces the initiating radicals; however, for the vast majority of photopolymerizable systems, this small difference in energy will be negligible compared to the contributions of heat of reaction and conduction to the overall energy balance. Also, note that the physical and thermal properties of the system (density, specific heat and conductivity) are assumed to remain constant throughout the course of the reaction.

2.2. The species balances

The species balances are slightly simpler than the energy balance, in that they each contain only three terms: accumulation, diffusion, and generation or consumption by reaction. The general species balance appears as

$$\frac{\mathrm{d}c_i}{\mathrm{d}t} = \frac{\mathrm{d}}{\mathrm{d}z}\left(\hat{c}D_i\frac{\mathrm{d}\hat{x}_i}{\mathrm{d}z}\right) + R_i, \tag{10}$$

where the subscript i refers to the species for which the equation is written (primary radicals, macroradicals, monomer, initiator, dead polymer, inhibitor or inhibited polymer chains). c_i represents the concentration of component i in the reacting mixture, D_i is the diffusion coefficient, and R_i is the reaction term, which comes from the reaction mechanism given by Eqs. (1)–(7).

The two variables with the overhats, c and x_i, warrant further explanation. For bulk polymerization, the polymer produced will have extremely low mobility, as entanglements will limit diffusion of the polymer after a few percent conversion has been reached. In crosslinking polymerizations, the polymer mobility will be essentially zero, as each monomer unit polymerized is incorporated into an all-encompassing network. Therefore, as a first approximation, macroscopic diffusion of polymeric species (including dead polymer, growing polymer chains, and inhibited polymeric chains) will be ignored, and the diffusive terms in the species balances on these components will be set to zero. Thus, the polymer matrix produced as the reaction proceeds will occupy space and reduce the concentrations of all the mobile species, without itself diffusing. Thus, the effective total concentration is the sum of the concentrations of all the mobile species (initiator, monomer, primary radicals and solvent), and the effective mole fraction of each diffusing species is the

concentration of that component divided by the effective total concentration. In mathematical form, these quantities are given by

$$\hat{c} = \sum_{\text{mobile}} c_i, \tag{11}$$

$$\hat{x}_i = \frac{c_i}{\hat{c}}. \tag{12}$$

For systems without solvent, the species balances described by Eq. (10) are solved for all species. When solvent is present, the species balances are solved for all reacting components, and the solvent concentration is determined by the overall mass balance. Assuming negligible volume shrinkage upon polymerization, the solvent concentration (c_S) can be found in each individual slice:

$$c_S = c_{\text{total}} - \sum_{\text{all } i} c_i, \tag{13}$$

where c_{total} is the sum of initial concentrations over all species, including solvent. Lastly, note that the form of Eq. (10) is written assuming equimolar counterdiffusion of the mobile species.

The assumption of negligible volume shrinkage warrants further discussion. Typically, a crosslinking system shows at most 10 percent volume shrinkage. Addition of an inert solvent will further reduce the degree of shrinkage. Thus, the systems simulated in this work will have relatively small degrees of volume shrinkage, which, in turn, will affect the overall concentrations very little. The uncertainties introduced by failing to capture actual volume reduction will be smaller than or, at worst, on the order of uncertainties of other parameters utilized in the model.

To compute properly the heat generation from light absorption and the fractional free volume (which lies at the heart of the diffusion-controlled kinetic constants, as indicated below), the total number of monomer and initiator moieties present in each slice must be known. The simplest way to achieve this is to write separate species balances for monomer and initiator which include only diffusion terms:

$$\frac{\mathrm{d}c_i^*}{\mathrm{d}t} = \frac{\mathrm{d}}{\mathrm{d}z}\left(\hat{c}D_i\frac{\mathrm{d}\hat{x}_i}{\mathrm{d}z}\right). \tag{14}$$

For example, when monomer leaves a slice by diffusion, the dummy variable c_M^* will be adjusted accordingly; but when monomer reacts through chain initiation or propagation, it will not effect the value c_M^*. Thus, the total number of monomer units, unreacted or incorporated into polymer, can be determined. This value is crucial in calculating the fractional free volume in a multi-component mixture. The same process allows the number of initiator units to be calculated. The value c_I^*, as previously mentioned, is used for calculating heat generated by light absorbance in the energy balance.

The remaining parameters to be determined are the diffusion coefficient for each species. As mentioned, the polymeric species are assumed to be immobile in the mixture, so the value of their diffusion coefficient is essentially zero. For the mobile components, a Doolittle-type equation is used to cast the diffusion coefficient of small molecules in terms of the fractional free volume of the mixture. Following Bueche (1962):

$$D_i = D_i^0 \mathrm{e}^{-A_i/f}. \tag{15}$$

D_i is the diffusion coefficient for component i, D_i^0 is the corresponding pre-exponential factor, A_i is a parameter which determines the rate of decrease of D_i with decreasing free volume, and f is the fractional free volume of the mixture.

2.3. Light intensity

The decrease in light intensity throughout the sample is calculated using the Beer–Lambert law. In this paper, only a non-photobleaching initiator will be considered, i.e., photolyzed initiator moieties retain the same absorbance as the original photoinitiator molecules. Furthermore, the diffusion of initiator and photolyzed initiator moieties is assumed to be negligible, and the light intensity profile does not change from its initial form. While these assumptions are not rigorously met in all polymerization scenarios, they do approximate the behavior in most conventional photopolymerized systems. With these assumptions, the Beer–Lambert law can be integrated with respect to sample depth, and the light intensity profile can be found explicitly:

$$I = I_0 \mathrm{e}^{-\varepsilon c_I^* z}. \tag{16}$$

In this equation, I is the light intensity at depth z into the sample, I_0 is the incident light intensity at the top surface of the sample, ε is the molar absorptivity of the initiator at the illuminating wavelength, and c_I^* is the instantaneous concentration of photoinitiator moieties. It should be noted that a similar expression can be written for photobleaching reactions, using the instantaneous concentration of the *unreacted* photoinitiator moieties to compute the instantaneous light intensity profile.

2.4. The kinetic constants

The form of the kinetic constants used in this work is similar to that used in the previously developed kinetic models (Goodner & Bowman, 1998, 1999), which were based upon the pioneering work of Marten and Hamielec (1978, 1982). They incorporate diffusion-controlled kinetics and termination by reaction diffusion, and are cast in terms of the fractional free volume of the polymerizing mixture. They differ from the previously presented forms in that they account for the temperature dependence of

the chemical reaction kinetic constants. The kinetic constants for propagation and termination appear as

$$k_p = \frac{k_{p0} e^{-E_p/RT}}{1 + e^{A_p(1/f - 1/f_{cp})}}, \tag{17}$$

$$k_t = k_{t0} e^{-E_t/RT} \times \left(1 + \frac{1}{(R_{rd} k_p [c_M]/k_{t0} e^{-E_t/RT}) + e^{-A_t(1/f - 1/f_{ct})}}\right)^{-1}. \tag{18}$$

In these equations, k_{p0} and k_{t0} are the pre-exponential factors for the true reaction kinetic constants (i.e., in the absence of diffusional limitations) for the propagation and termination reactions, respectively, and E_p and E_t are the activation energies for these chemical reactions. f_{cp} and f_{ct} are the critical fractional free volumes for propagation and termination. The physical significance of these parameters will be discussed later. A_p and A_t are parameters which determine the rate at which the kinetic constants decrease when diffusion-controlled. Other parameters appearing in the above equations are the universal gas constant, R, the local temperature, T, the reaction diffusion parameter, R_{rd}, and the instantaneous local double bond concentration, $[c_M]$.

The kinetic constants for most of the other reactions—chain initiation, reinitiation, and primary radical termination—will have a form identical to Eq. (17) with the appropriate subscripts. The one exception is the kinetic constant for inhibition. Since the inhibitor simulated in this work is molecular oxygen, a small and extremely mobile molecule, it is assumed that the critical free volume for the inhibition reaction will be exceedingly small compared to the free volume of the polymerizing mixture. Thus, the expression for the inhibition kinetic constant will be simplified to read

$$k_z = k_{z0} e^{-E_z/RT}, \tag{19}$$

where k_{z0} is the pre-exponential factor and E_z is the activation energy. In the case of an added inhibition compound having more mobility restrictions than oxygen, an equation having the form of Eq. (17) could easily be used for k_z.

The free volume is calculated using the same procedure as the previous kinetic models; the fractional free volume of the mixture is the volume average of the fractional free volumes of the individual components. However, in a system that has solvent present, the direct relation between free volume and conversion breaks down. Neglecting the free volume contribution of very low concentration components, such as initiator, primary radicals, inhibitor, and macroradicals, the set of equations describing the free volume in terms of the species concentration is

$$v_T = \frac{c_S M_S}{\rho_S} + \frac{c_M M_M}{\rho_M} + \frac{(c_M^* - c_M) M_M}{\rho_p}, \tag{20}$$

$$\phi_S = \frac{c_S M_S}{\rho_S v_T}, \tag{21}$$

$$\phi_M = \frac{c_M M_M}{\rho_M v_T}, \tag{22}$$

$$\phi_P = \frac{(c_M^* - c_M) M_M}{\rho_P v_T}, \tag{23}$$

$$f = 0.025 + \sum_{S,M,P} \phi_i \alpha_i (T - T_{gi}). \tag{24}$$

In these equations, ϕ_i represents the volume fraction of the indicated component, M_i is the molecular weight of that component, ρ_i is the density, and c_i is the concentration of the given component in the reaction mixture (with c_M^* as described previously). It should be noted that the volume fractions would normally be calculated using Eqs. (21)–(23) with v_T omitted. However, in these equations, v_T is included as a normalizing factor to assure the volume fractions sum to unity, thereby mitigating the imprecision introduced by uncertainties in values such as the polymer density, which may not be reported for proprietary formulations, or the (average) monomer molecular weight in complex mixtures. In Eq. (24), T_{gi} is the glass transition temperature of the pure component and 0.025 is assumed to be the fractional free volume of each component at its glass transition temperature. Note that when the concentration of solvent is zero, introducing the conversion through the equation $X = (c_M^* - c_M)/c_M^*$ gives the free volume correlation for a monomer/polymer mixture used in the previous kinetic models (Marten & Hamielec, 1978, 1982).

The physical significance of the critical free volumes for propagation and termination warrants further explanation. The value f_{cp} is the fractional free volume at which the reaction resistance for the chemical reaction ($1/k_r$, where k_r is the numerator in Eq. (17)) is equal to the reaction resistance for the diffusion process ($1/k_d$, where k_d is proportional to the diffusivity of the monomer given by Eq. (15)). In other words, at fractional free volumes greater than f_{cp}, the chemical reaction is the rate-limiting step in the overall propagation process; below f_{cp}, diffusion of monomer to the reactive site is the rate-limiting step in the process. Similar arguments belie the significance of the critical free volume for termination.

Understanding the origins of the critical free volumes and the relationship between reaction and diffusion allows the variation of critical free volume with temperature to be determined. By setting $1/k_r$ (the reaction resistance due to the chemical reaction) equal to $1/k_d$ (the reaction

Table 1
The parameters used in the comprehensive kinetic model are listed along with the reference from which the value was obtained or calculated. Unless indicated, monomer values refer to 2-hydroxyethyl methacrylate (HEMA), solvent values are for glycerine, and initiator properties are for 2,2-dimethoxy-2-phenylacetophenone (DMPA). For values that were not available for the HEMA/glycerine system, the parameters were estimated from similar formulations, and this information is shown in the remarks column[a]

Parameter	Value	Units	Ref.	Remarks
$[M]_0$	8.2	mol/l		
MW_m	130.14	g/mol		
MW_s	92.09	g/mol		
R	4	l/mol	Goodner et al.	
α_M	0.0005	$1/^\circ C$	Goodner et al.	
α_P	0.000075	$1/^\circ C$	Goodner et al.	
α_S	0.0005	$1/^\circ C$		Same as α_M
ρ_M	1.073	g/ml	Aldrich	
ρ_P	1.15	g/ml	Goodner et al.	
ρ_S	1.261	g/ml	Aldrich	
T_{gm}	213	K	Goodner et al.	
T_{gp}	328	K	Goodner et al.	
T_{gs}	173	K		Estimated
ϕ	0.6		Goodner et al.	
ε	150	l/mol c	Goodner et al.	
k_{p0}	1.6×10^6	l/mol s	Goodner et al.	
E_p	18.23×10^3	J/mol	Gao and Penlidis	For MMA
A_p	0.66		Goodner et al.	
f_{cp}	0.042		Goodner et al.	
k_{t0}	3.6×10^6	l/mol s	Goodner et al.	
E_t	2.94×10^3	J/mol	Gao and Penlidis	For MMA
A_t	1.2		Goodner et al.	
f_{ct}	0.060		Goodner et al.	
k_{i0}	1.6×10^6	l/mol s		Same as k_{p0}
k_{z0}	52.8×10^9	l/mol s	Odian	For O_2/MMA
k_{tp0}, k'_{i0}	0.0	l/mol s		Unless otherwise noted
E_i, E_z, E'_i	18.23×10^3	J/mol		Same as E_p
E_{tp}	2.94×10^3	J/mol		Same as E_t
A_i, A_{tp}, A'_i	0.66			Same as A_p
A_z	0.287			Calculated from diffusivity
f_{ci}, f_{ctp}, f'_{ci}	0.042		Goodner et al.	Same as f_{cp}
f_{cz}	0.010		Goodner et al.	Estimated
ΔH	-5.48×10^4	J/mol	Cook	From −13.1 kcal/mol
k	0.292	W/cm	Lide	For glycerine
ρc_p	1900	J/l K	Gao and Penlidis	Monomer/polymer average
D_{i0}	23.6×10^{-3}	cm^2/s	Lide	Small species in ethyl acetate
D_{m0}	23.6×10^{-3}	cm^2/s	Lide	Small species in ethyl acetate
D_{z0}	49.1×10^{-3}	cm^2/s	Brandrup and Immergut	O_2 in ethyl methacrylate

[a]The references refer to Goodner et al. (1997), Gao and Penlidis (1996), Odian (1991), Cook (1992), Lide (1993), and Brandrup and Immergut (1989).

resistance due to diffusion) at the critical free volume (f_c), the following expression is obtained:

$$k_0 e^{-E/RT} K e^{-A/f_c}. \tag{25}$$

In this equation, K includes the diffusivity pre-exponential factor and the proportionality between k_d and D. Note that the subscripts are dropped, as this equation can apply to propagation, termination, or any other diffusion-controlled kinetic process.

If the critical free volume is known at a single temperature, Eq. (25) can be used to determine the value of the constant K in terms of that free volume (f_c^{ref}), the temperature (T^{ref}), and the values of A, E, and k_0. Plugging the value of K thus obtained back into Eq. (25) renders an expression for the critical free volume as a function of temperature:

$$\frac{1}{f_c} = \frac{1}{f_c^{\text{ref}}} + \frac{E}{AR}\left(\frac{1}{T} - \frac{1}{T^{\text{ref}}}\right). \tag{26}$$

The variation of the critical free volumes for propagation and termination, using the model parameters given in Table 1, is shown in Fig. 1. As the temperature of the polymerizing mixture rises, both critical free volumes increase. The increase in the critical free volume for propagation is much greater than that of the termination process, as the activation energy for the propagation reaction is much higher. Without further explanation, it may

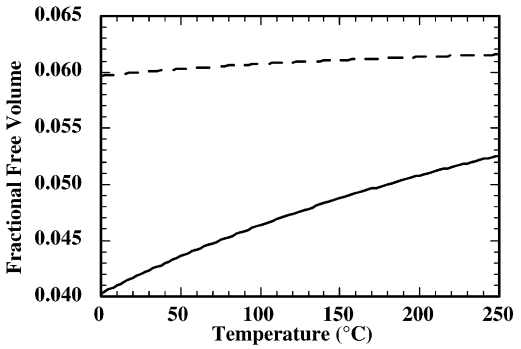

Fig. 1. Variation of critical fractional free volumes with temperature. The solid line indicates the critical free volume for propagation (f_{cp}), and the dashed line shows the critical free volume for termination (f_{ct}). The functional form of the two curves is given by Eq. (26).

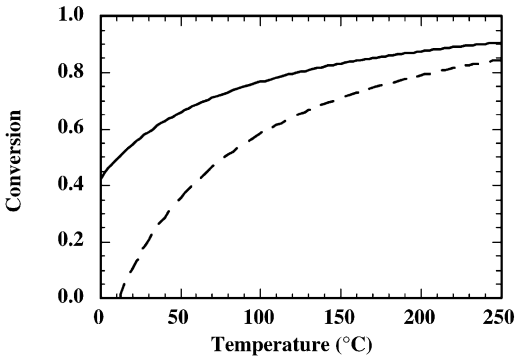

Fig. 2. Variation of critical conversion with temperature corresponding to the critical free volumes presented in Fig. 1. The solid line indicates the critical conversion for propagation, and the dashed line shows the critical conversion for termination.

seem counter-intuitive that the critical free volume increases with temperature. This behavior can be clarified, though, by examining the conversion at which the critical free volume occurs for different polymerization temperatures.

The conversions at which the propagation and termination processes become diffusion-controlled are plotted in Fig. 2. As the temperature of the polymerizing mixture is increased, the reaction proceeds to higher conversions before diffusional limitations begin to influence the reaction kinetics. So, even though Fig. 1 indicates that the critical free volumes increase with temperature, these conditions occur at higher conversions. As a result, when the temperature is increased, diffusion-controlled kinetics do not become predominant until later in the reaction, as expected. Also, note that at low temperatures (below 12°C), the termination reaction is diffusion-limited from the start of the polymerization. This feature is due to the increased viscosity of the monomer and the accompanying decrease of the macroradical mobility.

Another way to examine the relationship between the critical free volume and temperature is to plot the values

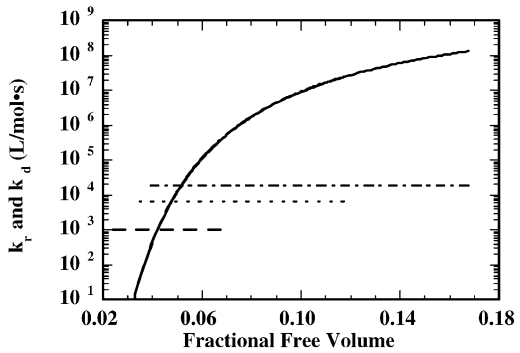

Fig. 3. The inverse reaction resistances, k_r and k_d, plotted as a function of fractional free volume for the propagation reaction. The solid line shows k_d, which is proportional to the diffusivity, as given by Eq. (15). The three horizontal lines correspond to k_r, the true chemical reaction kinetic constant, at three different temperatures: 25°C (dashed), 125°C (dotted), and 225°C (dash-dot).

of k_r (the true reaction kinetic constant) and k_d (the apparent reaction kinetic constant due to diffusion). These values are shown in Fig. 3. The kinetic constant due to diffusion, $k_d = K\exp(-A/f)$, increases monotonically as the free volume of the reacting mixture increases, and is not directly dependent upon temperature (other than the inherent relationship between free volume and temperature). The value of k_r $(= k_{r0}\exp(-E/RT))$ appears as a horizontal line that is dependent upon temperature only; i.e., at a given temperature, the value of k_r is fixed, irrespective of the free volume of the system. The point at which these two curves cross represents the critical free volume. At higher free volumes (corresponding to lower conversions), k_r is less than k_d, and propagation is reaction-controlled. At free volumes lower than the critical free volume, k_d is less than k_r. Thus, diffusion becomes the rate-limiting step in the propagation process at higher conversions. As the temperature of the system is increased, the value of k_r increases, which shifts the crossing point of the two curves to the right. Thus, the critical free volume increases with temperature, as indicated in Fig. 1.

2.5. Boundary conditions

While the differential equations specified in Eqs. (10), (11), and (14) are necessary to give the behavior of the species concentrations and temperature during the polymerization process, the problem is not completely specified without the proper boundary conditions. The thermal boundary conditions used in this work are either perfectly conducting or perfectly insulating. The conducting boundary condition simulates polymerization in contact with a highly thermally conductive substrate, such as a metal, or contact with air when there is sufficient heat removal by convection. This condition is imposed by holding the temperature of the boundary element

constant at the environment temperature. The adiabatic condition mimics contact with a low thermal conductivity substance, such as glass or plastic. It is specified by setting the first spatial derivative of temperature equal to zero at the top and/or bottom surfaces. While the true boundary conditions of any system are neither perfectly conducting nor perfectly insulating, some conditions come close to these specifications, and all possible boundary conditions will fall within the range bounded by these two. Additionally, the thermal boundary conditions can be set independently for the top and bottom surfaces.

The species concentration boundary conditions specified are generally no-flux across the top and bottom surfaces. This condition is met by setting the first spatial derivative of the mole fractions equal to zero and the top and bottom surfaces. The one exception with regard to the no-flux boundary condition is for the inhibitor. In the case of atmospheric oxygen diffusing into a sample, an oxygen flux must be allowed. Several methods could be used to specify the oxygen flux into the film (or the oxygen content in the top of the film), such as the definition of a Henry's Law constant or the specification of the steady-state solubility or concentration of oxygen in the system. For this work, the latter method was chosen, and the concentration of oxygen is specified as constant in the surface element. This method assumes that the solubility of oxygen in the monomer/polymer matrix does not change significantly over the course of the reaction but introduces the fewest number of adjustable parameters. As with the thermal boundary conditions, the no-flux and constant concentration boundary conditions on the inhibitor species can be independently specified at the top and bottom surfaces.

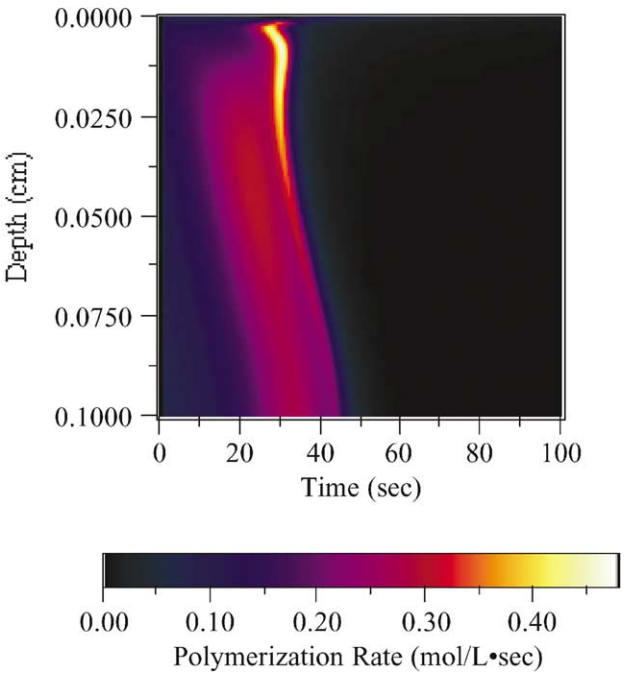

Fig. 4. Polymerization rate as a function of time and depth into the sample for a typical photopolymerization. The top boundary is perfectly conducting, while the lower surface is insulated. The sample thickness is 1 mm, the incident light intensity is 10 mW/cm^2, and the photoinitiator concentration is 0.1 M (corresponding to 22 percent light transmission through the sample). Initial oxygen concentration is 10^{-6} M, and oxygen is allowed to penetrate the top surface.

2.6. Model parameters

To simulate 'typical' polymerization behavior, a monomer commonly used in photopolymerization processes must be identified as a model compound. For this study, 2-hydroxyethyl methacrylate (HEMA) was chosen due to its prevalence in photopolymeric materials such as contact lenses. The majority of the kinetic and physical parameters for HEMA have been determined previously (Goodner, Lee, & Bowman, 1997). A 'typical' solvent must also be identified; for this study, solvent parameters represent glycerine, the solvent used in the polymerization of soft contact lenses. Values not known for the HEMA/glycerine system were estimated from values for similar methacrylate systems, such as methyl methacrylate or ethyl methacrylate, and are indicated as such. Other sources for kinetic and materials parameters are Aldrich Chemical Company (Milwaukee, WI), the Polymer Handbook (Brandrup & Immergut, 1989), the Handbook of Chemistry and Physics (Lide, 1993), and a commercial software package (WATPOLY) developed by Gao and Penlidis (1996). Table 1 lists all the kinetic and physical parameters used in this study and the particular source from which each parameter was obtained.

3. Results and discussion

Typical polymerization behavior in thick samples is shown in Figs. 4–6. In Fig. 4, the polymerization rate is shown as a function of depth and time for the polymerization of a 1 mm thick sample. Several interesting effects occur due to the sample thickness and boundary conditions. First, the attenuation in light intensity throughout the sample leads to a reduced rate of polymerization in the depths of the sample, along with a delay in the time at which the maximum rate occurs. In contrast to the isothermal results presented previously (Goodner & Bowman, 1998), the inclusion of heat generation from reaction and light absorbance along with heat transfer leads to an increased rate of polymerization before autoacceleration sets in. This increased rate is due to both an increase in the kinetic constant for the propagation reaction and a delay in the onset of autoacceleration, which results from increased molecular mobility at the elevated temperatures.

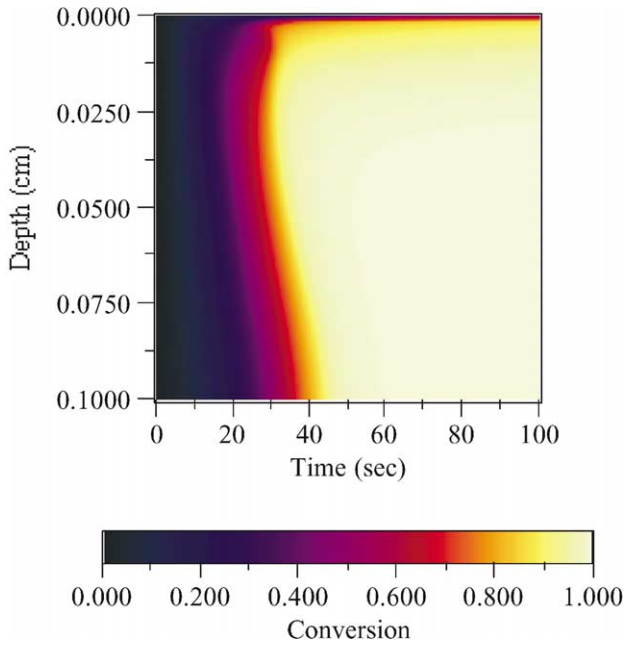

Fig. 5. Double bond conversion as a function of time and depth for the polymerization shown in Fig. 4.

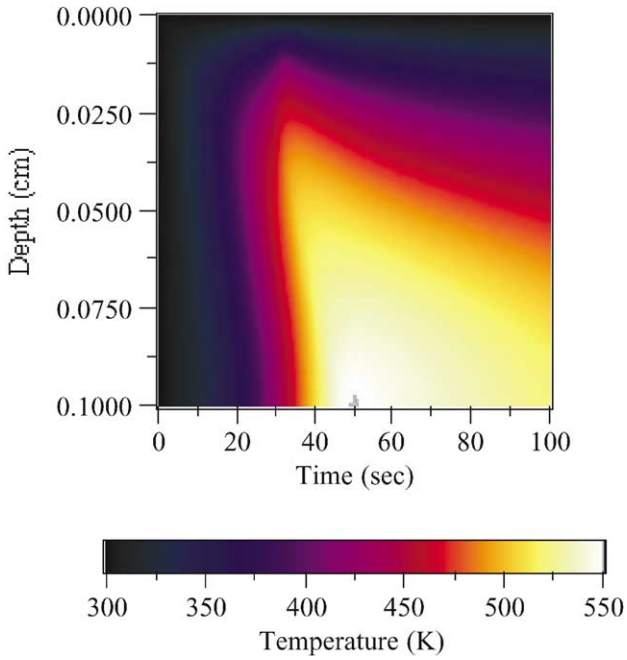

Fig. 6. Temperature profile in degrees kelvin for the polymerization shown in Fig. 4.

The thermal boundary conditions also contribute to the non-ideal polymerization behavior. At the top surface, which is conducting, the time to reach the maximum rate is characterized by a sharp decrease and a subsequent sharp (but not as abrupt) increase with depth into the film. These features can be explained through the effect of temperature on the free volume and the propagation kinetic constant. At the top surface, the temperature is specified to be 25°C by the boundary condition. Slightly into the film (where the decreased time to maximum rate occurs), a slight temperature increase leads to increased propagation, and therefore, consumption of monomer. Higher conversions are reached slightly faster, which in turn leads to a quicker onset of autoacceleration. Farther into the film, the temperature increase is larger. In addition to increasing the propagation kinetics, the free volume of the mixture is increased. This leads to a delay in the onset of autoacceleration through an increase in the critical free volume for termination, as predicted by Eq. (26) and shown in Fig. 2. This effect persists throughout the rest of the film, as the insulated boundary condition at the bottom surface has little effect other than retaining heat generated by the reaction. At this relatively high rate of initiation, the effects of oxygen inhibition on the polymerization rate are rather hard to discern, other than the reduction in rate during the first few seconds of polymerization.

The conversion profile for the same polymerization is shown in Fig. 5. Other than the features outlined in discussion of the polymerization rate profile, two effects are particularly noticeable in the conversion profile. First, the overall conversion reached is exceedingly high, approaching and even achieving full conversion of double bonds throughout most of the film. This phenomenon is due to the increased temperature throughout the sample, which serves to increase both the propagation kinetics and the molecular mobility. Thus, when autodeceleration is finally reached, nearly all of the double bonds in the system have reacted, and the few remaining double bonds can react before the polymerization rate becomes vanishingly small. The second noticeable feature in the conversion profile is that there is a thin layer of unreacted monomer at the top surface of the film. This layer is due to oxygen inhibition from the surrounding atmosphere; as oxygen is continually being replenished at the top surface, polymerization cannot progress to any significant degree. However, because of the relatively high rate of initiation, oxygen is consumed in a very thin skin and cannot penetrate appreciably into the bulk of the film.

The last figure, Fig. 6, concerning this "typical" polymerization shows the temperature profile during the polymerization. In addition to keeping the top portion of the film relatively cool throughout the polymerization, the conducting boundary condition at the top surface serves to remove heat from the bulk of the sample after the reaction has finished. While a good portion of the film reaches temperatures upwards of 250°C, the temperature begins to drop throughout the expanse of the film after the reaction ceases. It is interesting to note that while the increased temperatures afforded by the insulated bottom

boundary mitigate the decrease in rate caused by the attenuation of light intensity, the high temperatures reached may char, depolymerize, or otherwise damage the final polymeric material produced in such a reaction.

Before examining particular aspects of photopolymerization in thick films, a brief description of experimental measurement techniques is in order. Currently, the most prevalent way to determine polymerization kinetics is by monitoring the reaction using either differential scanning calorimetry (DSC) or infrared techniques, such as real-time IR or Fourier-transform IR. In these methods, a single value such as heat release (for DSC; representing rate of double bond consumption) or absorbance (for IR; providing double bond concentrations) is provided as a function of time. However, Figs. 4–6 clearly demonstrate that there is a wealth of complex behavior occurring throughout the depth of the film; the common DSC and IR methods provide merely an average behavior. While the average behavior is an important first step in characterizing the polymerization kinetics, kinetic modeling that incorporates spatial variations will provide unique insight into the complexities of the actual polymerization behavior, at least until spatially resolved reaction monitoring methods become more common for free-radical photopolymerization.

Now that the utility of the comprehensive kinetic model has been demonstrated in predicting rate, conversion, and temperature profiles over the course of a polymerization, the effect of various parameters and conditions will be explored in more detail. In the following examinations, profiles will be presented as functions of either depth or time to present the magnitude of the values more clearly. For the data plotted as a function of time, a convention will be used to minimize specific edge effects (such as those seen in Fig. 4) while capturing the polymerization behavior near the top or bottom of the film. When a profile is indicated as being at the "top" of the sample, it refers to the profile taken 10 percent of the depth from the top surface of the sample. Likewise, the "bottom" of the sample represents the profile 10 percent from the bottom surface of the film. For instance, if profiles show the conversion at the top and bottom of a 3 mm thick sample, the data shown is the conversion at depths of 0.3 and 2.7 mm. If the goal is to indeed capture the edge effects and show the data at the true top or bottom, the figure and accompanying discussion will indicate that the profile shows the "top surface" or "bottom surface".

The first effect to be examined in detail is the influence of the thermal boundary conditions and heat transfer on the polymerization rate, conversion, and temperature. Fig. 7 shows polymerization rate profiles near the top of a 3 mm thick sample. The isothermal profile shows typical diffusion-controlled polymerization behavior, with three distinct regions: non-diffusion limited polymerization, autoacceleration after 50 s, and autodeceleration after 80 s. While this kinetic behavior is typical of thin films in contact with conducting surfaces, neglecting the heat production by reaction and the subsequent transfer of that heat eliminates the complex polymerization behavior seen in thick films.

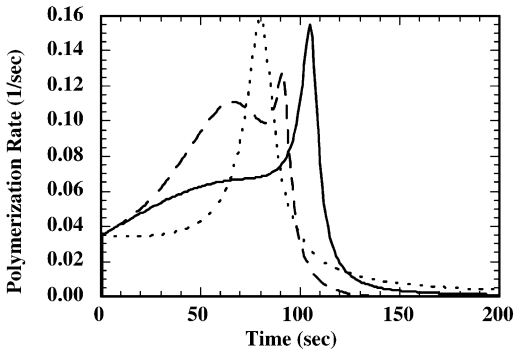

Fig. 7. Normalized polymerization rate profiles near the top of a 3 mm thick sample for the first 200 s of polymerization. The solid line indicates conducting boundary conditions, the dashed line is insulated boundaries, and the dotted line is the isothermal case. Light intensity is 1 mW/cm^2, and initiator concentration is 0.1 M (giving 1.1 percent transmittance). No inhibitor is present.

The simulation performed with conducting boundaries predicts similar, but not identical, rate behavior. Instead of a nearly constant rate at the beginning of the reaction, the temperature rise due to the exothermic reaction causes an increase in the propagation kinetic constant along with a concomitant rise in the rate of polymerization. This increase slowly levels off after 60 s, as the increase in k_p is countered by the decrease in the double bond concentration as monomer is consumed. Autoacceleration is delayed until 90 s. This delay results from an increase in the free volume, and thus the mobility, of the system due to the increased temperature. Thus, higher conversions can be reached before the termination reaction becomes diffusion limited.

The polymerization performed with insulated boundary conditions appears as an exaggeration of the conducting case. The initial rise in polymerization rate due to increasing temperature is even more pronounced, as the adiabatic top and bottom surfaces trap the heat generated by reaction. Because of the greatly increased rate and consequent monomer consumption, low monomer concentration leads to the downturn in rate seen at 60 s. This drop persists until 80 s, at which point the termination reaction becomes diffusion-controlled and autoacceleration sets in. Thus, two rate maxima are seen during the polymerization, the first thermally induced, and the second caused by autoacceleration. Note that the autoacceleration peak is reduced in both amplitude and area; this feature results from the lower concentration of unreacted monomer at the start of autoacceleration.

Fig. 8 shows the temperature profiles associated with the polymerization shown in Fig. 7. As expected, a greater temperature rise results in the film insulated at

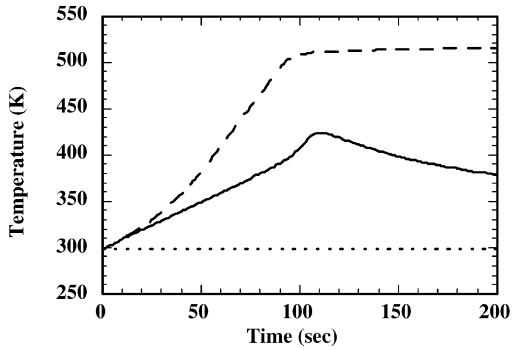

Fig. 8. Temperature profiles in the top of the sample for the polymerization shown in Fig. 7. Conducting boundary condition is indicated by the solid line, insulating boundaries by the dashed line, and the isothermal case (dotted line) is shown for reference.

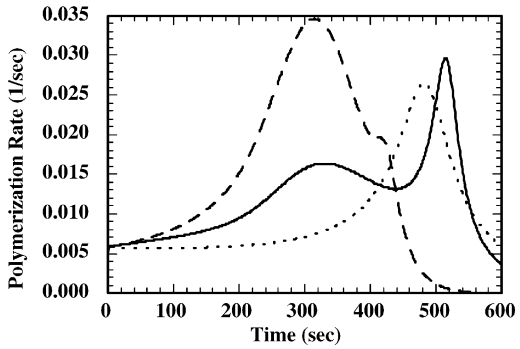

Fig. 10. Normalized rate profiles at the bottom of the sample for the polymerization shown in Fig. 7. The solid line indicates conducting boundary conditions, the dashed line is insulated boundaries, and the dotted line is the isothermal case. Note the change in scales on both time and rate. Light intensity at this point in the sample is 0.017 mW/cm^2.

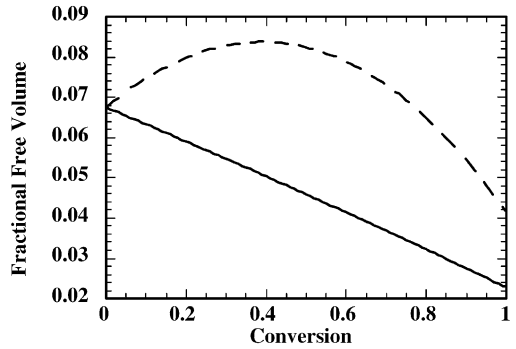

Fig. 9. The variation of fractional free volume with conversion. The solid line indicates the variation in an isothermal system. The dashed line shows the effect of the temperature rise due to the exothermic reaction in an adiabatic system. The initial temperature for both scenarios is 25°C.

both the top and bottom. The conducting boundary case also shows the effect of autoacceleration on the heat production. After a steady increase in temperature over the first 100 s of polymerization, the temperature shoots up 30° in only a few seconds. After the polymerization rate drops, the temperature begins to decrease as thermal conduction transports heat to the boundaries and out of the film.

In the above discussion, the increase in mobility afforded by increased temperatures was referred to. This behavior is shown explicitly in Fig. 9. In this figure, two cases are shown. The solid line shows the variation of free volume with conversion in the polymerizing mixture for an isothermal system. The free volume steadily decreases as monomer is converted into polymer, going from a value of 0.068 at the start of the reaction to 0.022 at full conversion, which is well below the critical free volumes for both propagation and termination. However, when the system is adiabatic, the heat generated by reaction causes the free volume to actually increase over the first 40 percent conversion. As the reaction proceeds further, the free volume decreases, but only to 0.041 at full conversion. In a more direct comparison of the two cases, the critical free volume for termination (0.060 at 25°C) is reached after only 18 percent conversion in the isothermal system, but over 80 percent conversion must be reached before the adiabatic system shows diffusion-controlled termination, even when accounting for the rise in the critical free volume predicted by Eq. (26).

Whereas Fig. 7 showed the polymerization rate at the top of a 3 mm thick film, Fig. 10 gives the corresponding rate profiles at the bottom of the film. The rate behavior is qualitatively similar to that seen at the top of the film, with several differences. First, the maximum polymerization rates reached are reduced by approximately a factor of four at the bottom of the sample, and the times required to reach the maximum rate are increased by nearly the same ratio. The rate peaks are also accordingly broadened. These features reflect the reduction in light intensity penetrating to the depths of the film and the resultant decrease in the rate of initiation.

The reduction in overall rate also leads to a change in the shape of the conducting and insulated systems' rate profiles. While the rate is decreased for the conducting boundary system, the extended time scale of the polymerization allows enough monomer to be consumed that the rate starts to drop after 330 s. The rate continues to drop until a high enough conversion is reached that autoacceleration sets in at 450 s, giving two rate maxima. The adiabatic case also shows a change in the rate profile. Because the temperature increases monotonically in the system, the propagation kinetic constant continues to increase, and a relatively large amount of monomer is consumed during the thermally induced rate maximum centered at 310 s. By the time autoacceleration commences, there is very little monomer left. This leaves the autoacceleration rate maximum insignificant when compared to the thermal rate maximum.

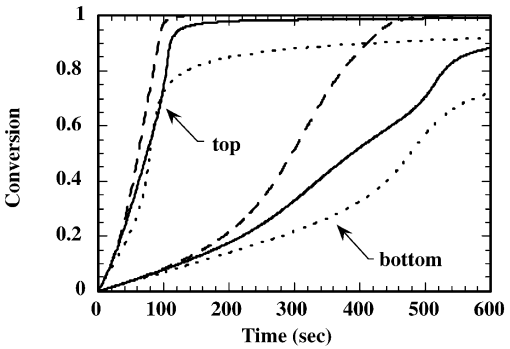

Fig. 11. Conversion profiles in the top and bottom of the sample for the polymerization shown in Fig. 7. The solid lines indicate conducting boundary conditions, the dashed lines are for the insulated boundaries, and the dotted lines are for the isothermal case.

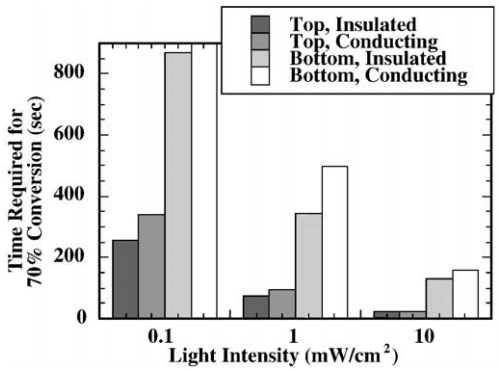

Fig. 12. Time required to reach 70 percent conversion as a function of light intensity. The data for the bottom of a film with a conducting boundary condition at the low light intensity exceeds the scale of the figure; its actual value is 1705 s.

Fig. 11 shows the conversion profiles corresponding to Figs. 7 and 10. The greatest conversion is reached in the adiabatic system, as the increased temperature provides the extra mobility required to achieve complete conversion. The conducting case reaches nearly the same conversion at the top of the film, with a slight reduction because of the heat lost through the boundaries. However, at the bottom of the film, the conducting system profile lags far behind the adiabatic system. This effect results from a combination of the thermal boundary conditions and the low light intensity at the bottom of the film. In the adiabatic system, the increase in propagation is sufficient to offset the low radical concentration, which results from the attenuated light intensity. In the conducting system, however, the temperature increase is much smaller due to heat transfer. As a result, the overall conversion is considerably decreased. The isothermal case shows the lowest conversions at both the top and bottom of the film. Because there is no rise in temperature to provide extra mobility as in the previous cases, the isothermal system reaches a maximum conversion of approximately 92 percent. Some monomer remains unreacted but trapped in the polymeric matrix. This result is significant in systems in which unreacted monomer can pose toxicity or other problems.

The next effect examined is the influence of the light intensity on conversion in a thick sample. Fig. 12 depicts the time required to reach 70 percent conversion in the top and at the bottom of a 3 mm thick sample. In addition to showing the decrease in processing time required to reach a specified conversion as the light intensity is increased, the data displays the importance of accounting for heat transfer and light intensity effects in a thick sample. For instance, if the cure time required for 70 percent conversion at 1 mW/cm^2 light intensity were predicted using a homogeneous model, the model results would indicate a polymerization of around 100 s to be sufficient. However, at the bottom of the film, far longer times are required to reach the given conversion, and the 100 s cure predicted by the homogeneous model would result in a product well below the desired specifications. Furthermore, the comprehensive model shows that the thermal boundary conditions significantly effect the cure time required to achieve the desired conversion at the bottom of the film. The greater temperature rise afforded by the adiabatic system increases the polymerization rate, and the reaction takes less than 350 s to reach 70 percent conversion. The conducting system does not reach the specified cure until another 150 s have passed. Also note that the difference in polymerization time between the insulated and conducting systems increases as the light intensity is decreased. The slower polymerization rates at the low light intensities allow for more heat to be lost to the environment in the conducting system, resulting in a smaller temperature rise, and hence, a much slower polymerization in comparison to the adiabatic system.

4. Conclusions

In this work, a comprehensive kinetic model to simulate polymerization in thick samples was developed. The model allows light intensity, temperature, and species concentration to vary across the thickness of a photopolymerized film. Heat generation by reaction and light absorption are included, as is heat transfer by conduction. Mass transfer is accounted for by allowing equimolar counterdiffusion of small molecules in the reacting mixture. In addition to diffusion-controlled propagation and termination kinetics, primary radical termination and inhibition mechanisms are incorporated into the model.

Model predictions are used to elucidate the effects of different environmental parameters on the polymerization rate, conversion, and temperature in both thick and thin samples. It is shown that heat generation and heat transfer can greatly influence the polymerization rate in thick samples. Retention of heat in thick samples leads to final

conversions approaching 100 percent, as the extra mobility and increased propagation kinetics afforded by the increased temperatures allows the reaction to proceed to greater extents than displayed in isothermal systems. The heat generated by reaction can also lead to two maxima in the rate profile. The first is due to increased propagation at high temperatures; the second is the autoacceleration peak normally seen in diffusion-controlled polymerizations. Heat generation also facilitates greater polymerization at the bottom of thick samples, somewhat mitigating the lower initiation rates with increased propagation kinetics. It is also shown that adiabatic boundary conditions result in faster and more complete curing; however, these increases are somewhat offset by the increased temperatures, which can damage the final product.

References

Anseth, K. S., & Bowman, C. N. (1993). Reaction diffusion enhanced termination in polymerizations of multifunctional monomers. *Polymer Reaction Engineering*, *1*, 499–520.

Anseth, K. S., Newman, S. M., & Bowman, C. N. (1995). Polymeric dental composites: properties and reaction behavior of multimethacrylate dental restorations. *Advances in Polymer Science*, *122*, 177–217.

Brandrup, J., & Immergut, E. H. (Eds.) (1989). *Polymer handbook*. New York: Wiley.

Broer, D. J., Mol, G. N., & Challa, G. (1991). Temperature effects on the kinetics of photoinitiated polymerization of dimethacrylates. *Polymer*, *32*, 690–695.

Buback, M. (1990). Free-radical polymerization up to high conversion. A general kinetic treatment. *Die Makromolekulare Chemie*, *191*, 1575–1587.

Buback, M., Huckestein, B., & Russell, G. T. (1994). Modeling of termination in intermediate and high conversion free radical polymerizations. *Macromolecular Chemistry and Physics*, *195*, 539–554.

Bueche, F. (1962). *Physical properties of polymers*. New York: Interscience.

Cook, W. D. (1992). Thermal aspects of the kinetics of dimethacrylate photopolymerization. *Polymer*, *33*, 2152–2161.

Decker, C. (1996). Photoinitiated crosslinking polymerisation. *Progress in Polymer Science*, *21*, 593–650.

Decker, C., & Elzaouk, B. (1995). Laser curing of photopolymers. In N. S. Allen, M. Edge, I. R. Bellobono, & E. Selli (Eds.), *Current trends in polymer photochemistry* (pp. 130–148). New York: Ellis Horwood.

Decker, C., Faure, J., Fizet, M., & Rychla, L. (1979). Elimination of oxygen inhibition in photopolymerization. *Photographic Science and Engineering*, *23*, 137–140.

Decker, C., & Jenkins, A. D. (1985). Kinetic approach of O_2 inhibition in ultraviolet- and laser-induced polymerizations. *Macromolecules*, *18*, 1241–1244.

Gao, J., & Penlidis, A. (1996). A comprehensive simulator/database package for reviewing free-radical homopolymerizations. *Journal of Macromolecular Science—Reviews in Macromolecular Chemistry and Physics*, *C36*, 199–404.

Goodner, M. D., & Bowman, C. N. (1998). Modeling and experimental investigation of light intensity and initiator effects on solvent-free photopolymerizations. In T. E. Long, & M. O. Hunt (Eds.), *Solvent-free polymerizations and processes: Minimization of conventional organic solvents*. (Vol. 713) (pp. 220–231). Washington, DC: American Chemical Society.

Goodner, M. D., & Bowman, C. N. (1999). Modeling primary radical termination and its effects on autoacceleration in photopolymerization kinetics. *Macromolecules*, *32*, 6552–6559.

Goodner, M. D., Lee, H. R., & Bowman, C. N. (1997). Method for determining the kinetic parameters in diffusion-controlled free-radical homopolymerizations. *Industrial and Engineering Chemistry Research*, *36*, 1247–1252.

Kannurpatti, A. R., Peiffer, R. W., Guymon, C. A., & Bowman, C. N. (1996). Photochemistry of polymers: Photopolymerization fundamentals and applications. In R. A. Lessard, & W. F. Frank (Eds.), *Critical reviews of optical science and technology: Polymers in optics: Physics*, *chemistry*, *and applications* (Vol. CR63) (pp. 136–163). Bellingham, WA: SPIE Optical Engineering Press.

Kloosterboer, J. G. (1988). Network formation by chain crosslinking photopolymerization and its applications in electronics. *Advances in Polymer Science*, *84*, 1–61.

Kloosterboer, J. G., van de Hei, G. M. M., Gossink, R. G., & Dortant, G. C. M. (1984). The effects of volume relaxation and thermal mobilization of trapped radicals on the final conversion of photopolymerized diacrylates. *Polymer Communications*, *25*, 322–325.

Lide, D. R. (Ed.) (1993). *Handbook of chemistry and physics.* Boca Raton, FL: CRC Press.

Marten, F., & Hamielec, A. (1978). High conversion diffusion-controlled polymerization. In J. Henderson, & T. Bouton (Eds.), *Polymerization reactors and processes* (Vol. 104) (pp. 43–69). Washington, DC: American Chemical Society.

Marten, F. L., & Hamielec, A. E. (1982). High-conversion diffusion-controlled polymerization of styrene. I. *Journal of Applied Polymer Science*, *27*, 489–505.

Odian, G. (1991). *Principles of polymerization*. New York: Wiley.

Panke, D. (1995). Modelling the free-radical polymerization of methyl methacrylate over the complete range of conversion. *Macromolecular Theory and Simulation*, *4*, 759–772.

Peiffer, R. W. (1997). Applications of photopolymer technology. In A. B. Scranton, C. Bowman, & R. Peiffer (Eds.), *Photopolymerization: fundamentals and applications* (Vol. 673) (pp. 1–14). Washington, DC: American Chemical Society.